

## Supporting Information

**Zhao et al.**

### SI Text

**SI Materials and Methods. *Preparation of cisplatin crosslinked DNA.*** To activate cisplatin, 5  $\mu\text{M}$  cis-diamminedichloroplatinum(II) (Sigma-Aldrich, St. Louis, MO, USA) was incubated with 6.25  $\mu\text{M}$   $\text{AgNO}_3$  for 16 h at 295 K in the dark. The resulting  $\text{AgCl}$  was sedimented by twice centrifuging at 15,000 g for 10 min and the supernatant that contained the activated cisplatin was recovered. For site-specific incorporation of cisplatin, each oligonucleotide with a single pair of adjacent guanines was mixed with a 1.3-fold molar excess of activated cisplatin in 100 mM ammonium acetate ( $\text{NH}_4\text{Ac}$ ) buffer (pH 6.0) and incubated overnight at 310 K in the dark. The crosslinked products were purified by reverse-phase HPLC on a Vydac 218TP1010 (C18) column using a linear gradient of 12.5-50 % (v/v) methanol in 40 mM  $\text{NH}_4\text{Ac}$  (pH 6.0) followed by TBE-urea gel electrophoresis when needed. Finally, oligos were mixed with complementing strands in a 1:1 ratio and annealed by heating to 368 K and slow-cooling to room temperature.

***Crystallization and structure determination.*** Protein expression, purification and crystallization were carried out as described previously (1). Crystals were grown by the hanging-drop vapor-diffusion method, and the optimized reservoir buffer contained 0.1 M MES (pH 6.0), 5 mM  $\text{MgCl}_2$ , and 19-21% (w/v) PEG 2K-MME. After several rounds of streak and microseeding, diffraction-quality crystals grew to maximal dimensions over 3-7 days. Diffraction data were collected at SER-CAT in APS, processed with HKL2000 (2) or XDS (3) and converted to structure factors using TRUNCATE (4). Refinement and structure analysis were performed using COOT (5), PHENIX (6) and PyMOL ([www.pymol.org](http://www.pymol.org)).

***Kinetic measurement.*** The primer extension assay and steady-state  $K_m$  and  $k_{\text{cat}}$  measurement were carried out using normal or cross-linked template and 5'-fluorescein labeled primer, whose sequences are shown in Fig. 1B and Fig. S5. The W297A mutant was made using QuikChange Site-Directed Mutagenesis Kit (Stratagene) and purified as

for WT hPol  $\eta$ . For the reaction, typically 2.5 – 17 nM Pol  $\eta$  were incubated with 5  $\mu$ M primer-template substrate and various concentrations of deoxynucleoside triphosphates (dNTP) (0-200  $\mu$ M for kinetic measurements and 0-2000  $\mu$ M for dATP inhibition) in 40 mM Tris-HCl (pH 7.5), 5 mM MgCl<sub>2</sub>, 10 mM dithiothreitol, 100 mM KCl, 0.1 mg/ml bovine serum albumin, and 5% glycerol. Reactions were carried out at room temperature for 4 or 8 min and terminated by the addition of 10X formamide loading buffer (80% deionized formamide, 10 mM EDTA, pH 8.0, 1 mg/ml xylene cyanol). After denaturation by heating at 90°C for 3 min and immediate cooling on ice, reaction products were resolved on 20% polyacrylamide sequencing gels containing 5.5 M urea. Quantification and curve fitting were carried out as previously described (7).

## References

1. Biertümpfel C, *et al.* (2010) Structure and mechanism of human DNA polymerase  $\eta$ . *Nature* 465(7301):1044-1048.
2. Otwinowski Z, Minor W (1997) Processing of X-ray diffraction data collected in oscillation mode. *Methods Enzymol.* 276:307-326.
3. Kabsch W (2010) XDS. *Acta Crystallographica Section D* 66:125-132.
4. CCP4 (1994) The CCP4 suite: programs for protein crystallography. *Acta Crystallogr. D* 50:760-763.
5. Emsley P, Cowtan K (2004) Coot: model-building tools for molecular graphics. *Acta Crystallogr D Biol Crystallogr* 60(Pt 12 Pt 1):2126-2132.
6. Adams PD, *et al.* (2010) PHENIX: a comprehensive Python-based system for macromolecular structure solution. *Acta Crystallogr D Biol Crystallogr* 66(Pt 2):213-221.
7. Wang F, Yang W (2009) Structural insight into translesion synthesis by DNA Pol II. *Cell* 139(7):1279-1289.
8. Wong JH, *et al.* (2010) Structural insight into dynamic bypass of the major cisplatin-DNA adduct by Y-family polymerase Dpo4. *Embo J* 29(12):2059-2069.
9. Alt A, *et al.* (2007) Bypass of DNA lesions generated during anticancer treatment with cisplatin by DNA polymerase  $\eta$ . *Science* 318(5852):967-970.
10. Silverstein TD, *et al.* (2010) Structural basis for the suppression of skin cancers by DNA polymerase  $\eta$ . *Nature* 465(7301):1039-1043.

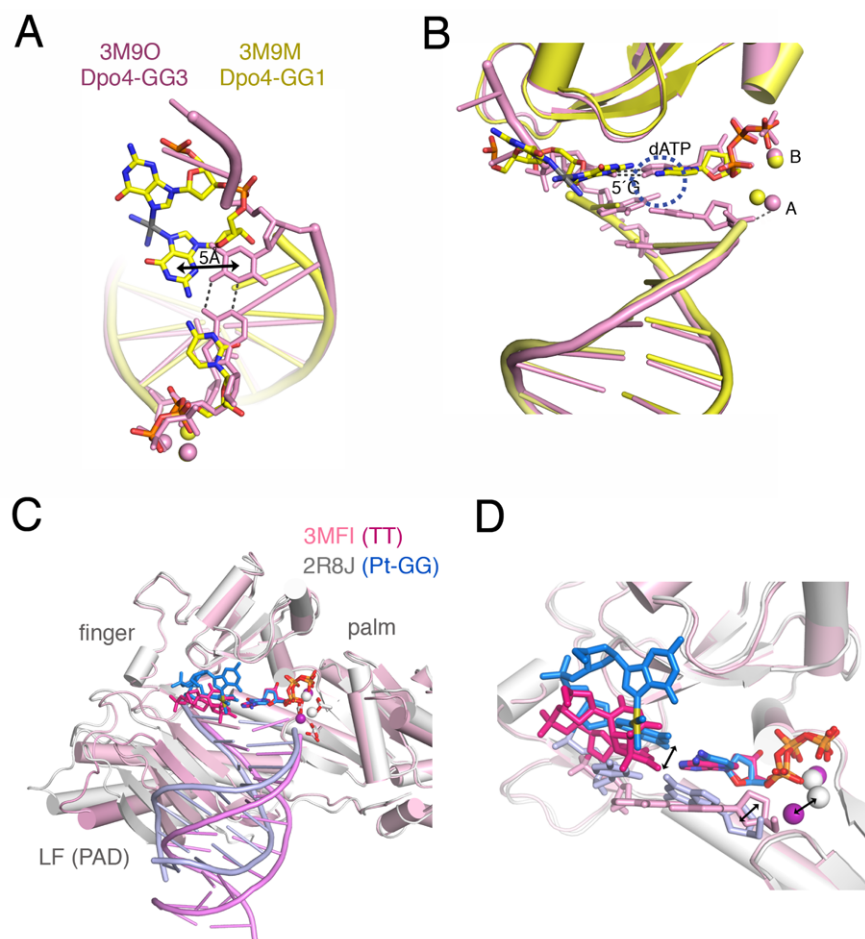


**Fig. S1.** The structures of Dpo4 and yeast Pol  $\eta$  complexed with Pt-GG. (A) Comparison of the replicating-base position in Dpo4 GG1 (PDB: 3M9M, yellow) and GG3 (3M90, pink) (8). Relative to the normal templating position (3M90), the 3'G of Pt-GG in Dpo4-GG1 is shifted by 5Å to outside of the active site as indicated. (B) An orthogonal view from A showing the absence of the 3'-nucleotide of the primer in Dpo4-GG1 due to disorder. In Dpo4-GG3, the 5'G has close contact with the dATP as indicated by the blue dashed circle. In both structures, the A-site metal ion is coordinated to the phosphate rather than the 3'-OH at the primer end. (C, D) Comparison of the inactive yeast Pol  $\eta$  complexed with Pt-GG (PDB: 2R8J, grey and blue) (9) and the active yeast Pol  $\eta$  with a thymine dimer (3MFI, pink) (10). The active site residues, the incoming nucleotide, and the palm and finger domains are roughly superimposable. But the LF (PAD) and the DNA duplexes differ by 3Å. (D) A close-up view of the active site. The displacement of the templating base, the primer 3'-end and the A-site metal ion are indicated by black double arrows.

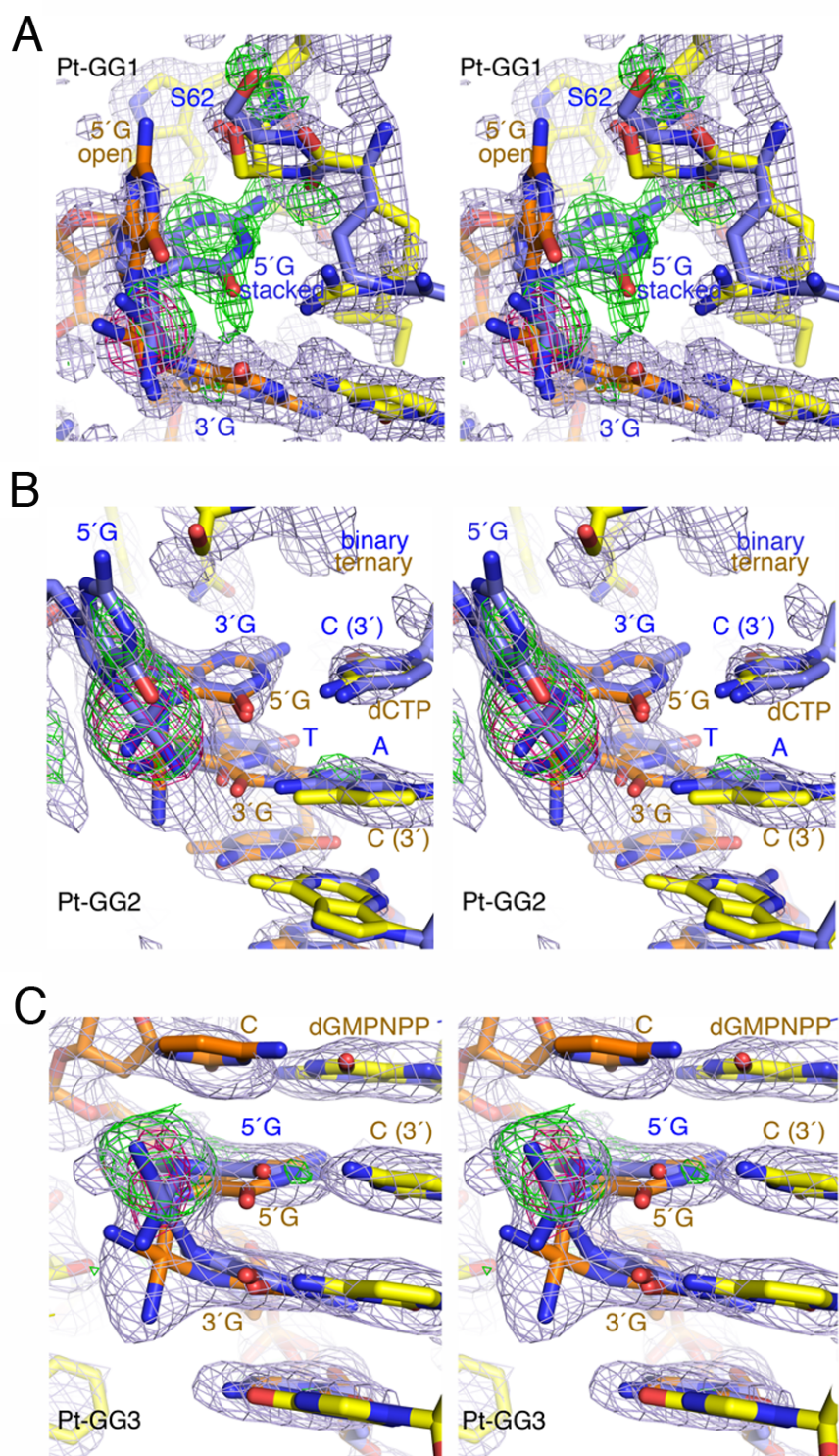


**Fig. S2.** Evidence of two DNA conformations in Pt-GG1, Pt-GG2 and Pt-GG3. (A) 2Fo-Fc ( $1.0 \sigma$ , blue mesh) and Fo-Fc map ( $2.8 \sigma$ , green mesh for positive peaks) calculated from the open conformation of Pt-GG (orange sticks) in Pt-GG1 reveals the 5'G stacked-in conformation of Pt-GG (blue sticks). The two conformations of S62 are also evident. Anomalous maps ( $3.0 \sigma$ , pink mesh) for platinum are also included. (B) 2Fo-Fc ( $1.0 \sigma$ ) and Fo-Fc map ( $2.8 \sigma$ ) calculated from the ternary complex alone (yellow / orange sticks) reveals strong uninterpreted densities around Pt-GG. Additional Fo-Fc peaks are found between base pairs, which can be explained by a second population of DNA (blue sticks, the binary complex). (C) 2Fo-Fc ( $1.0 \sigma$ ) and Fo-Fc ( $2.8 \sigma$ ) map calculated from one conformation in Pt-GG3 (orange sticks), which has close contacts with the dGMPNPP, reveals the second conformation of Pt-GG (blue sticks). All panels show stereo views.

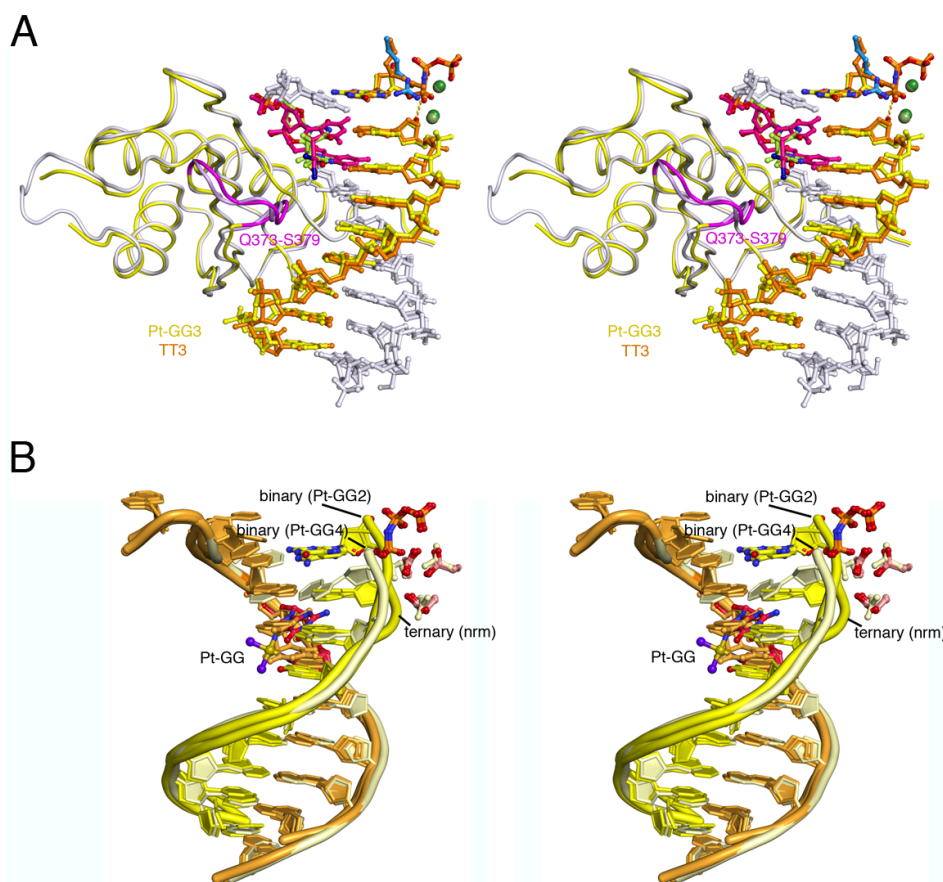


**Fig. S3.** Structural comparison of Pt-GG3 and Pt-GG4 with other hPol  $\eta$  binary and ternary complexes. (A) Stereo view of the DNA superposition of the Pt-GG3 (grey and yellow) and thymine dimer TT3 (PDB 3MR5, grey and orange) (1). The LF domains are included to show the slight outward shift in Pt-GG3 (yellow). The Q373-S379 loop (highlighted in magenta for Pt-GG3 and light purple for TT3) is similar in both structures and differs from others (Fig. 2A). (B) Stereo views of DNA superposition from the normal ternary complex (nrm, PDB 3MR2), TT4 (PDB 3MR6) (1), the product-mimic binary complex (Pt-GG2), and Pt-GG4 (binary, color in pale yellow with red Pt-GG). The DNAs in the ternary complexes are superimposable. But the 3' end of the primer strand differs significantly in the binary complex Pt-GG2 and Pt-GG4, and both differ from the ternary complexes. The active site carboxylates are shown in red sticks except for those in Pt-GG4, which are shown in pale yellow.

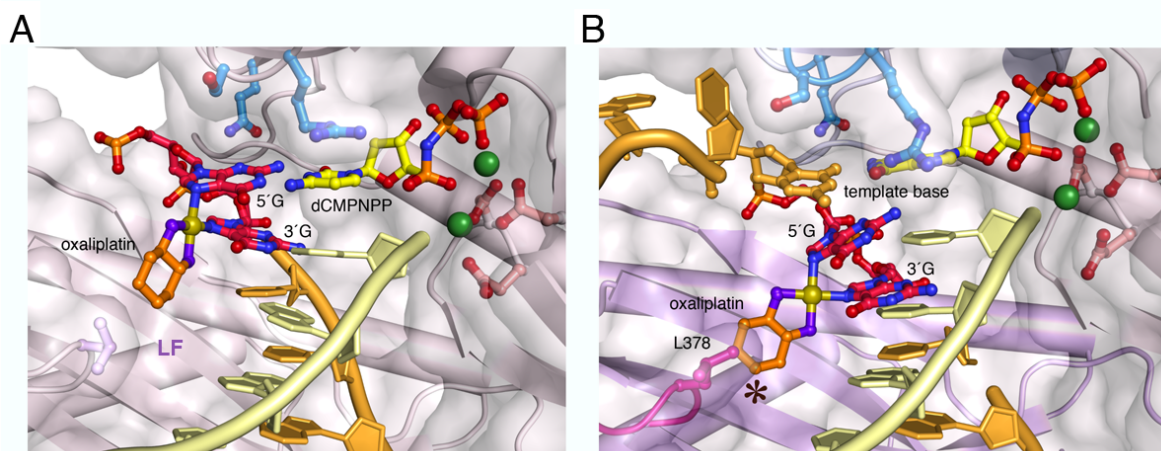


**Fig. S4.** Modeling of oxaliplatin bypass by hPol  $\eta$ . (A) Oxaliplatin is accommodated at the first and second nucleotide incorporation step by hPol  $\eta$ . The additional cyclohexane ring modeled onto the cisplatin is shown in orange and makes van-der-Waals contact with the LF. (B) Primer extension after the oxaliplatin lesion is difficult. The hexane moiety of the platinum adduct would clash with LF (colored in light purple), particularly with L378 in the Q373-S379 loop highlighted in magenta.

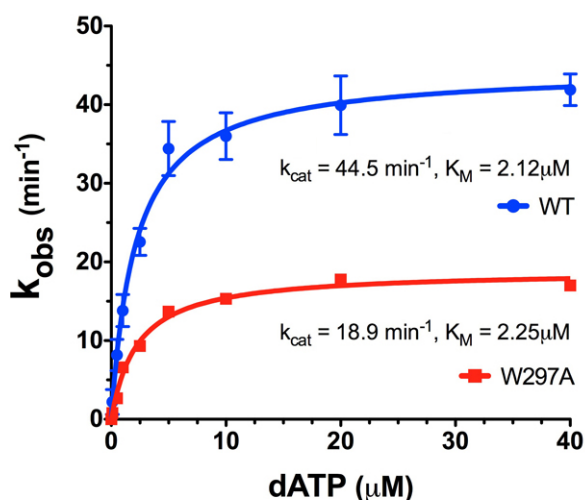


**Fig. S5.** Measurement of  $k_{cat}$  and  $K_M$  of WT and the W297 mutant hPol  $\eta$ . The oligos 5'-GAGTCATGTTTACGCTAGGCAC-3' and 5'-GTGCCTAGCGTAA-3' were used in the dATP incorporation and also the dATP inhibition assays (Fig. 6B). The reaction conditions were described in the SI Materials and Methods.

**Table S1. DNA oligos crystallized with hPol  $\eta$** 

Structure name	PDB code	DNA sequence		Incoming dNTP
GG0a	4DL2	3' TCACACTCGGCA 5' TAGTGTGAG	5' 3'	dCMPNPP
GG0b	4DL3	3' TCACACTGGCAT 5' TAGTGTGAC	5' 3'	dCMPNPP
Pt-GG1	4DL4	3' TCACACTCGGCA 5' TAGTGTGAG	5' 3'	dCMPNPP
Pt-GG2	4DL5	3' TCACACTGGCAT 5' TAGTGTGAC	5' 3'	dCMPNPP
Pt-GG3	4DL6	3' TCACACGGCTAT 5' TAGTGTGCC	5' 3'	dGMPNPP
Pt-GG4	4DL7	3' TCACTGGCTCAT 5' TAGTGACCG	5' 3'	dAMPNPP

GG (in red) denotes cisplatin crosslinked Pt-GG.

**Table S2. Kinetic parameters of dNTP incorporation by hPol  $\eta$** 

Template	dNTP	$K_M$ ( $\mu\text{M}$ )	$k_{\text{cat}}$ ( $\text{min}^{-1}$ )	$k_{\text{cat}}/K_M$ ( $\mu\text{M}^{-1}\text{min}^{-1}$ )	relative efficiency
Nrm-GG (averaged)	dCTP	$3.2 \pm 0.7$	$135 \pm 7.9$	42.2	1.00
Pt-GG1	dCTP	$3.1 \pm 0.2$	$107 \pm 2$	34.5	0.82
Pt-GG2	dCTP	$3.1 \pm 0.3$	$46 \pm 1$	14.8	0.35
Pt-GG3	dGTP	$15.5 \pm 0.6$	$132 \pm 1$	8.5	0.20
Pt-GG4	dATP	$8.0 \pm 0.9$	$10.0 \pm 0.3$	1.3	0.03
Pt-GG2	dATP	$71 \pm 13$	$10.6 \pm 0.6$	0.2	-
Nrm-GG1	dCTP	$2.5 \pm 0.2$	$145 \pm 3$	58.0	-
Nrm-GG2	dCTP	$5.3 \pm 0.3$	$168 \pm 3$	31.7	-
Nrm-GG3	dGTP	$2.5 \pm 0.1$	$171 \pm 2$	68.4	-
Nrm-GG4	dATP	$3.6 \pm 0.3$	$59 \pm 1$	16.4	-

**Table S3. Data collection and refinement statistics**

	GG0a (Nrm1)	GG0b (Nrm2)	Pt-GG1	Pt-GG2	Pt-GG3	Pt-GG4
PDB Code	4DL2	4DL3	4DL4	4DL5	4DL6	4DL7
<b>Data collection</b>						
Space group	P 6 <sub>1</sub>	P 6 <sub>1</sub>	P 6 <sub>1</sub>	P 6 <sub>1</sub>	P 6 <sub>1</sub>	P 6 <sub>1</sub>
Cell dimensions						
<i>a</i> , <i>b</i> , <i>c</i> (Å)	97.86	97.38	99.21	99.41	98.78	99.00
	97.86	97.38	99.21	99.41	98.78	99.00
	80.53	81.00	82.15	82.09	81.51	81.89
Wavelength (Å)	1.0000	1.0000	1.0000	1.0000	1.0000	1.0000
Resolution (Å)	30-2.15	30-2.10	30-2.00	30-2.92	30-2.50	30-1.97
<i>R</i> <sub>sym</sub> (%)	9.1 (53.7)	9.7 (55.1)	12.9 (58.1)	7.6 (68.4)	12.0 (70.5)	8.7 (40.5)
<i>I</i> / $\sigma$ <i>I</i>	17.9 (3.3)	12.7 (2.5)	11.3 (4.6)	18.9 (2.46)	7.3 (1.9)	12.0 (2.1)
Completeness (%)	99.5 (99.9)	98.6 (97.7)	99.7 (97.4)	99.7 (99.9)	97.8 (93.2)	97.8 (82.3)
Redundancy	6.0 (5.9)	3.9 (3.5)	4.5 (3.83)	4.8 (4.94)	2.7 (2.52)	3.7 (1.9)
<b>Refinement</b>						
Resolution (Å)	30-2.15	30-2.10	30-2.0	30-2.92	30-2.50	30-1.97
No. reflections	23814	25207	30539	10042	15461	31395
<i>R</i> <sub>work</sub> / <i>R</i> <sub>free</sub>	19.3/22.2	20.4/21.7	19.4/21.7	23.4/24.2	20.2/22.0	19.1/21.3
No. atoms						
Protein/DNA	3347/393	3366/393	3346/376	3276/373	3318/393	3339/393
Ligand/ion	48	48	36	30	33	17
Water	217	281	209	-	61	342
B-factors						
Protein/DNA	27.5/31.8	27.7/31.7	26.8/26.6	80.6/87.2	46.9/53.6	20.4/24.4
Ligand/ion	21.7	21.3	17.9	75.5	37.7	20.9
Water	27.9	28.1	30.2	-	42.6	24.6
R.m.s deviations						
Bond lengths (Å)	0.004	0.004	0.004	0.011	0.006	0.004
Bond angles (°)	0.849	0.751	0.997	1.204	1.175	0.815

\*Highest resolution shell is shown in parenthesis.